

Supporting Information

for

Lighting Up Hypochlorous Acid through C(sp²)-H Hydroxylation with a Solvatochromic Organoiridium(III) Probe

*Bhaskar Sen^a, Jogat Gogoi^a, Kripamoy Aguan^b, and Snehadrinarayan Khatua^{*a}*

^aDepartment of Chemistry, North Eastern Hill University, Shillong-793022,
Meghalaya.

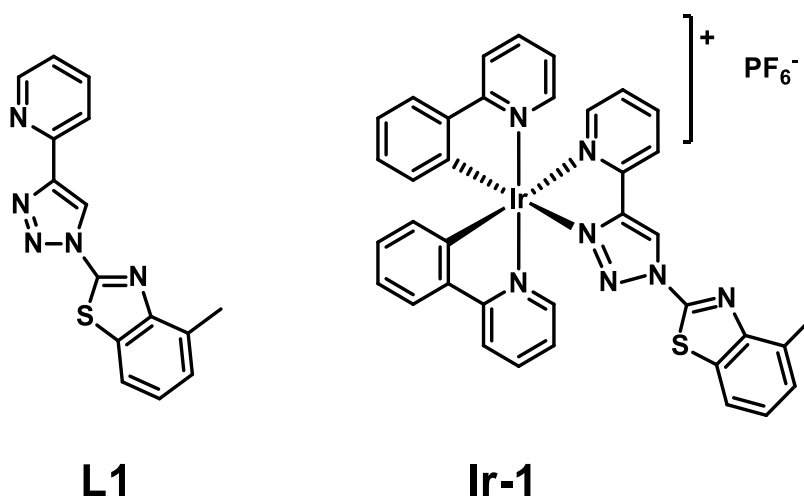
^bDepartment of Biotechnology and Bioinformatics, North Eastern Hill University,
Shillong-793022, Meghalaya

**Email: snehadri@gmail.com; skhatua@nehu.ac.in.*

Table of contents

SI No	Contents	Page No.
1.	List of compounds	S2
2.	NMR spectra of complex Ir-1	S3-S5
3.	ESI-HRMS spectra of complex Ir-1	S5
4.	Crystallographic data of Ir-1	S6-S9
5.	Normalized UV-vis and PL spectra of Ir-1 in PBS buffer	S9
6.	CIE coordinates of Ir-1 in various polar and nonpolar solvents	S10
7.	Selectivity and titration experiments of Ir-1 using UV-vis spectroscopy.	S10
8.	Titration spectra of Ir-1 for the calculation of LOD.	S11
9.	List of selected probes for HClO/CLO ⁻ detection	S11-S13
10.	Time-resolved emission decays of Ir-1 in the absence and presence of HOCl	S13
11.	Computational study and optimized structures	S14
12.	Bond properties of Ir-1 and Ir-1-OH .	S15
13.	Cartesian coordinates Ir-1 and Ir-1-OH in ground state.	S16-S17
14.	Theoretical calculation for transitions responsible for UV-vis absorption in Ir-1 using singlet state TD-DFT.	S18
15.	Cytotoxicity study	S19

Chart S1. List of compounds



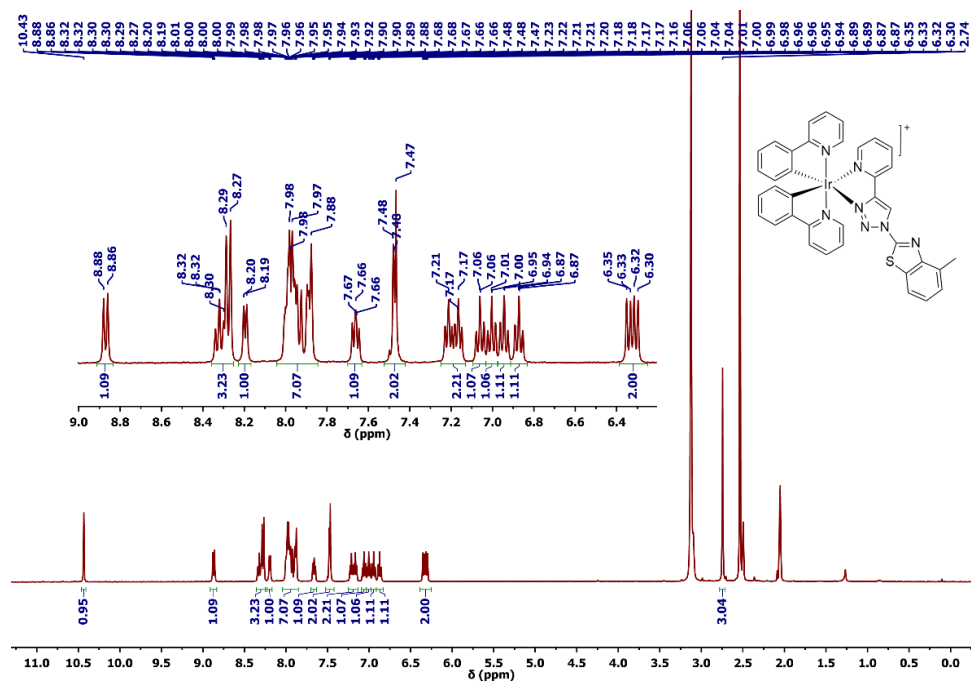


Fig. S1. ^1H NMR spectrum of Ir-1 in acetone- d_6 : DMSO- d_6 (v/v; 6:4).

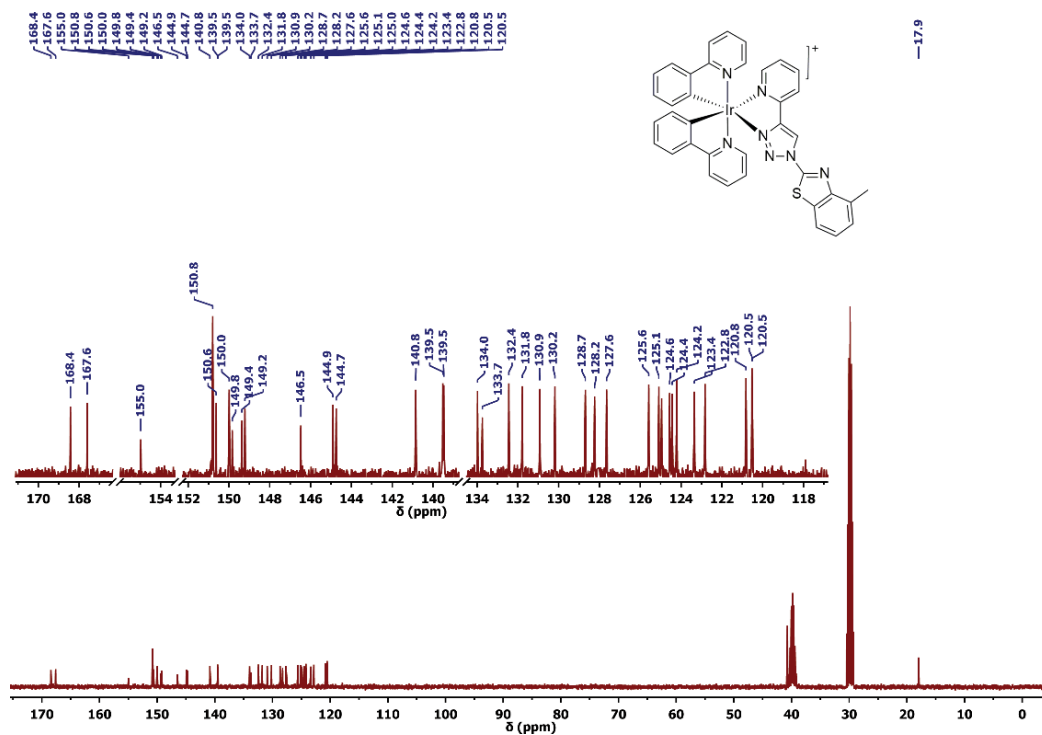


Fig. S2. ^{13}C NMR spectrum of Ir-1 in acetone- d_6 : DMSO- d_6 (v/v; 6:4)

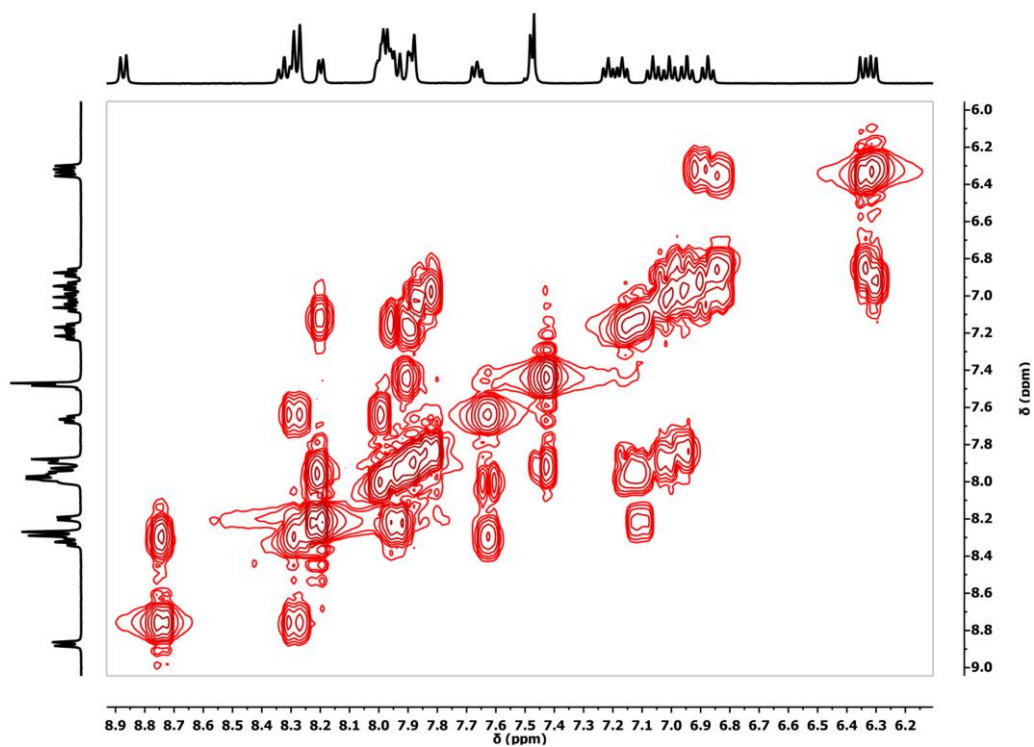


Fig. S3. Partial ^1H - ^1H COSY NMR spectrum of **Ir-1** in acetone- d_6 : DMSO- d_6 (v/v; 6:4).

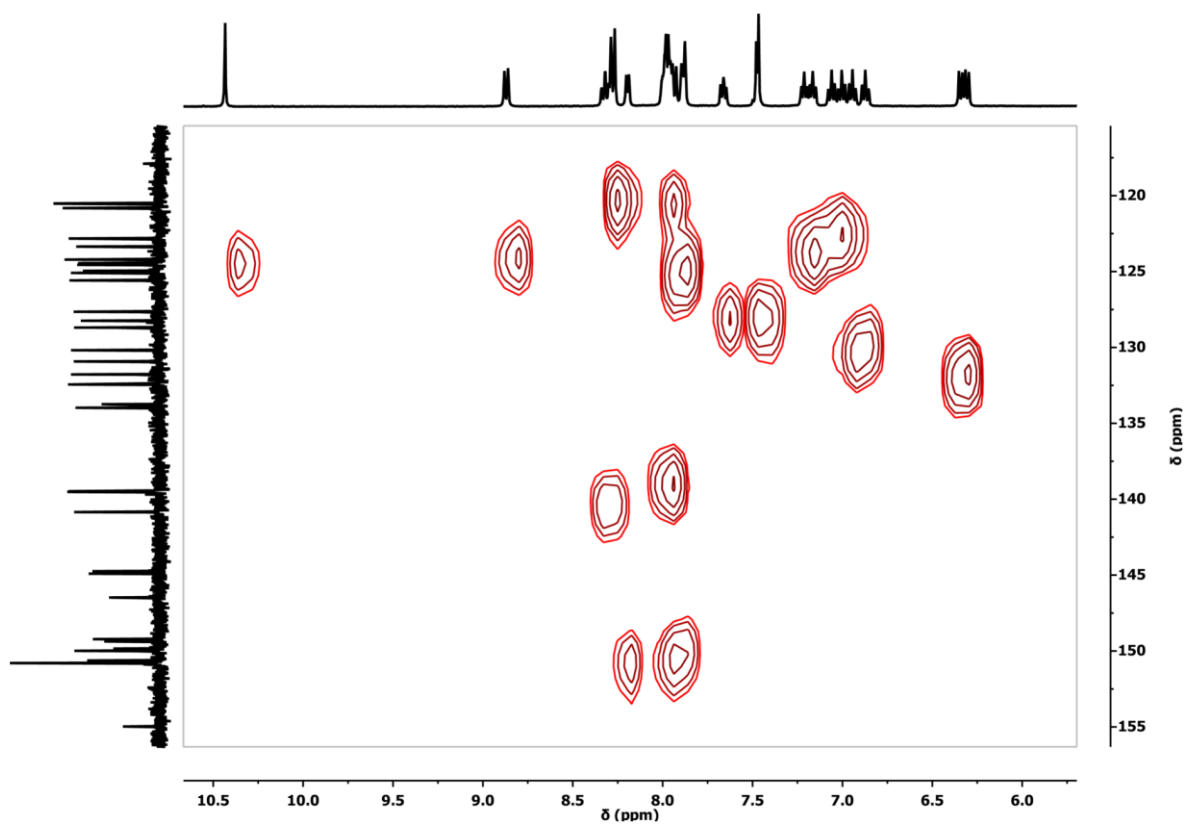


Fig. S4. Partial ^1H - ^{13}C HSQC NMR spectrum of **Ir-1** in acetone- d_6 : DMSO- d_6 (v/v; 6:4).

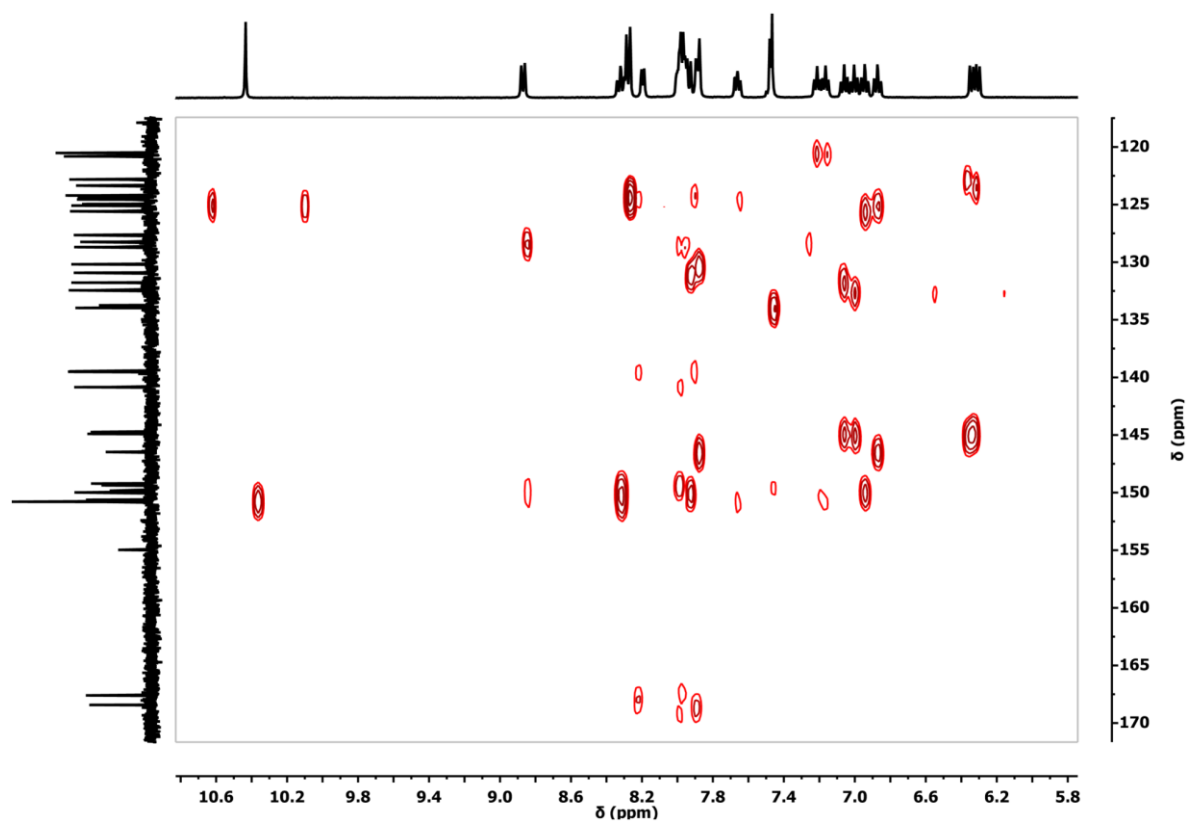


Fig. S5. Partial ^1H - ^{13}C HMBC NMR spectrum of **Ir-1** in acetone- d_6 : DMSO- d_6 (v/v; 6:4).

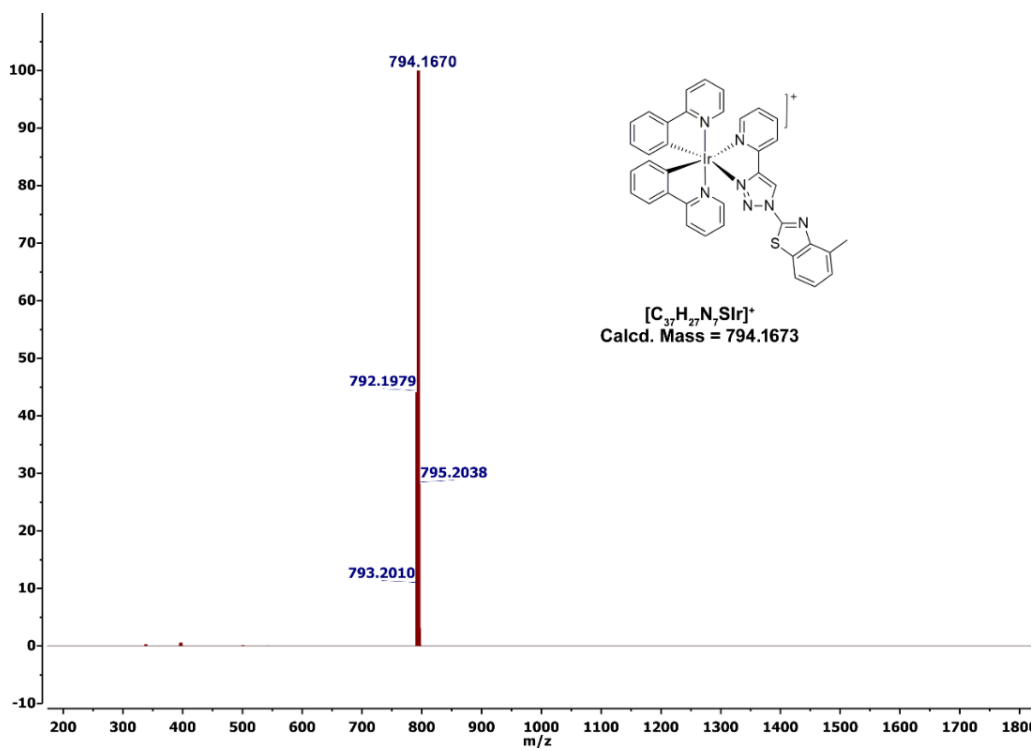


Fig. S6. ESI-HRMS spectrum of **Ir-1** in CH_3CN .

Table S1. Crystal data and structure refinement for **B**.

Empirical formula	C ₈ H ₆ N ₄ S	
Formula weight	190.23	
Temperature	293(2) K	
Wavelength	0.71073 Å	
Crystal system	Monoclinic	
Space group	C2/c	
Unit cell dimensions	$a = 16.8152(13) \text{ \AA}$	$\alpha = 90^\circ$.
	$b = 8.1255(4) \text{ \AA}$	$\beta = 122.810(11)^\circ$.
	$c = 14.3117(12) \text{ \AA}$	$\gamma = 90^\circ$.
Volume	1643.5(3) Å ³	
Z	8	
Density (calculated)	1.538 Mg/m ³	
Absorption coefficient	0.344 mm ⁻¹	
F(000)	784	
Crystal size	0.180 x 0.120 x 0.080 mm ³	
Theta range for data collection	3.387 to 26.365°.	
Index ranges	-20 ≤ h ≤ 19, -9 ≤ k ≤ 10, -14 ≤ l ≤ 17	
Reflections collected	2990	
Independent reflections	1669 [R(int) = 0.0145]	
Completeness to theta = 26.000°	99.4 %	
Absorption correction	Semi-empirical from equivalents	
Max. and min. transmission	0.973 and 0.941	
Refinement method	Full-matrix least-squares on F ²	
Data / restraints / parameters	1669 / 0 / 119	
Goodness-of-fit on F ²	1.076	
Final R indices [I > 2σ(I)] ^a	R1 = 0.0718, wR2 = 0.2113	
R indices (all data) ^a	R1 = 0.0821, wR2 = 0.2210	
Largest diff. peak and hole	0.730 and -0.375 e.Å ⁻³	

^a $R1 = \frac{\sum ||F_o| - |F_c||}{\sum |F_o|}$; $wR2 = \{\frac{\sum [w(F_o^2 - F_c^2)^2]}{\sum w(F_o^2)^2}\}^{1/2}$

Table S2. Bond lengths [\AA] and angles [$^\circ$] for **B**.

Bond lengths (\AA)			
C(1)-C(2)	1.378(5)	C(1)-C(6)	1.398(5)
C(1)-N(1)	1.416(4)	C(2)-C(3)	1.390(5)
C(2)-C(7)	1.530(4)	C(3)-C(4)	1.374(5)
C(4)-C(5)	1.380(5)	C(5)-C(6)	1.385(5)
C(6)-S(1)	1.746(3)	C(8)-N(4)	1.305(6)
C(8)-N(1)	1.352(5)	C(8)-S(1)	1.745(5)
N(1)-N(2)	1.341(5)	N(2)-N(3)	1.307(6)
N(3)-N(4)	1.380(7)		
Bond angles ($^\circ$)			
C(2)-C(1)-C(6)	123.3(3)	C(2)-C(1)-N(1)	126.5(3)
C(6)-C(1)-N(1)	110.2(3)	C(1)-C(2)-C(3)	115.5(3)
C(1)-C(2)-C(7)	118.4(3)	C(3)-C(2)-C(7)	126.0(3)
C(4)-C(3)-C(2)	122.0(3)	C(3)-C(4)-C(5)	121.9(3)
C(4)-C(5)-C(6)	117.6(3)	C(5)-C(6)-C(1)	119.7(3)
C(5)-C(6)-S(1)	126.9(3)	C(1)-C(6)-S(1)	113.4(2)
N(4)-C(8)-N(1)	109.6(4)	N(4)-C(8)-S(1)	137.2(4)
N(1)-C(8)-S(1)	113.1(3)	N(2)-N(1)-C(8)	109.0(3)
N(2)-N(1)-C(1)	136.9(3)	C(8)-N(1)-C(1)	114.1(3)
N(3)-N(2)-N(1)	105.1(4)	N(2)-N(3)-N(4)	111.9(4)
C(8)-N(4)-N(3)	104.3(4)	C(8)-S(1)-C(6)	89.20(18)

Table S3. Crystal data and structure refinement for **Ir-1**.

Empirical formula	C ₇₅ H ₅₆ C ₁₂ F ₁₂ Ir ₂ N ₁₄ P ₂ S ₂	
Formula weight	1962.69	
Temperature	293(2) K	
Wavelength	0.71073 Å	
Crystal system	Monoclinic	
Space group	I2/c	
Unit cell dimensions	$a = 23.1897(9)$ Å	$\alpha = 90.000(2)^\circ$.
	$b = 11.6878(4)$ Å	$\beta = 93.234(3)^\circ$.
	$c = 26.9335(8)$ Å	$\gamma = 90.000(5)^\circ$.
Volume	7288.3(4) Å ³	
Z	4	
Density (calculated)	1.789 Mg/m ³	
Absorption coefficient	3.909 mm ⁻¹	
F(000)	3848	
Crystal size	0.280 x 0.220 x 0.140 mm ³	
Theta range for data collection	2.256 to 23.634°.	
Index ranges	-26 ≤ h ≤ 19, -13 ≤ k ≤ 12, -20 ≤ l ≤ 30	
Reflections collected	10502	
Independent reflections	5472 [R(int) = 0.0402]	
Completeness to theta = 23.634°	99.8 %	
Absorption correction	Semi-empirical from equivalents	
Max. and min. transmission	0.745 and 0.555	
Refinement method	Full-matrix least-squares on F^2	
Data / restraints / parameters	5472 / 0 / 490	
Goodness-of-fit on F^2	1.052	
Final R indices [I > 2σ(I)] ^a	R1 = 0.0443, wR2 = 0.1183	
R indices (all data) ^a	R1 = 0.0631, wR2 = 0.1264	
Largest diff. peak and hole	1.741 and -1.512 e.Å ⁻³	

^a $R1 = \Sigma||F_o| - |F_c||/\Sigma|F_o|$; $wR2 = \{\Sigma[w(F_o^2 - F_c^2)^2]/\Sigma w(F_o^2)^2\}^{1/2}$

Table S4. Selected bond lengths (Å) and angles (°) around the Ir(III) center in **Ir-1**.

Bond lengths (Å)			
Ir(1)-N(7)	2.049(6)	Ir(1)-N(6)	2.070(6)
Ir(1)-N(2)	2.118(6)	Ir(1)-N(1)	2.176(6)
C(26)-Ir(1)	2.017(8)	C(37)-Ir(1)	2.011(8)
Bond angles (°)			
C(37)-Ir(1)-C(26)	89.8(3)	C(37)-Ir(1)-N(7)	80.5(3)
C(26)-Ir(1)-N(7)	95.9(3)	C(37)-Ir(1)-N(6)	95.1(3)
C(26)-Ir(1)-N(6)	80.0(3)	N(7)-Ir(1)-N(6)	174.0(2)
C(37)-Ir(1)-N(2)	96.7(3)	C(26)-Ir(1)-N(2)	172.3(3)
N(7)-Ir(1)-N(2)	89.3(2)	N(6)-Ir(1)-N(2)	95.3(3)
C(37)-Ir(1)-N(1)	172.3(3)	C(26)-Ir(1)-N(1)	97.3(3)
N(7)-Ir(1)-N(1)	95.8(2)	N(6)-Ir(1)-N(1)	89.0(2)
N(2)-Ir(1)-N(1)	76.5(2)		

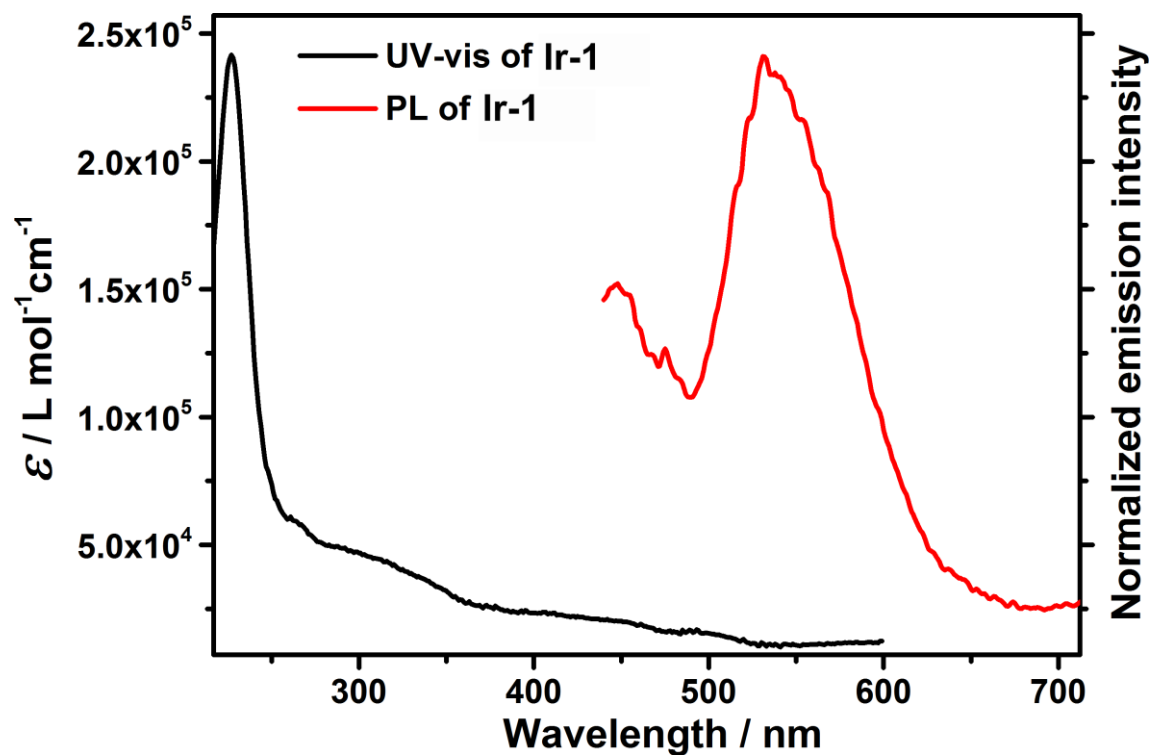


Fig. S7. UV-visible and normalized PL spectra of **Ir-1**.

Table S5. CIE coordinates of **Ir-1** in different solvents.

Sl no.	Medium	CIE coordinates (x,y)
1.	Hexane	0.24, 0.48
2.	Toluene	0.26, 0.50
3.	Ethyl ether	0.30, 0.55
4.	Dichloromethane	0.29, 0.54
5.	Tetrahydrofuran	0.30, 0.53
6.	Chloroform	0.27, 0.50
7.	Ethyl acetate	0.27, 0.50
8.	1,4-Dioxane	0.32, 0.52
9.	Acetone	0.35, 0.51
10.	Methanol	0.33, 0.48
11.	Ethanol	0.33, 0.51
12.	Acetonitrile	0.32, 0.47
13.	Dimethyl sulfoxide	0.33, 0.47
14.	Water	0.40, 0.42

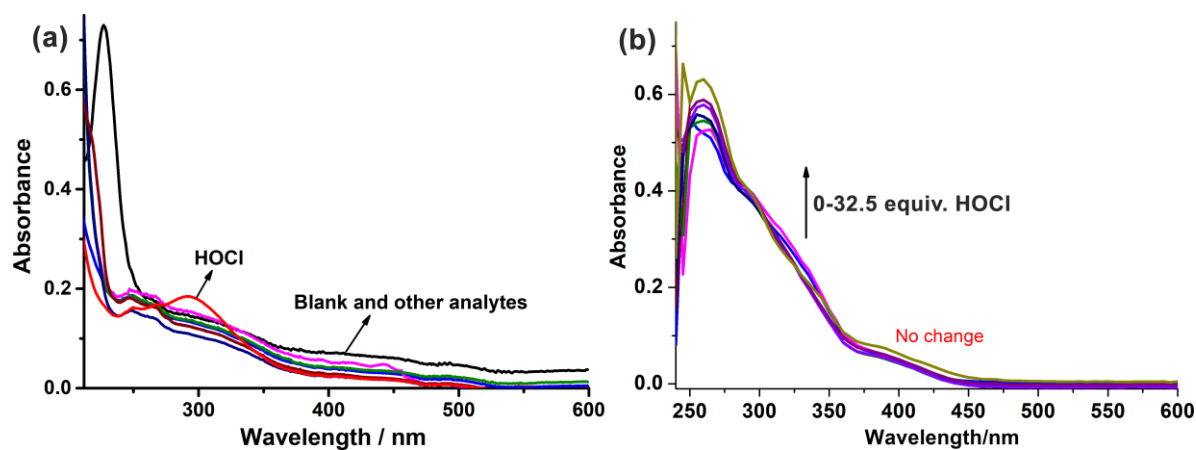


Fig. S8. (a) UV-visible selectivity of **Ir-1** (10 μ M) in the presence of various ROS/RNS and other anions in PBS buffer (DMSO: PBS, 1:1; v/v). (A-Q: Blank, AcO^- , OH^- , F^- , H_2PO_4^- , Cl^- , NO_3^- , CN^- , Br^- , I^- , H_2O_2 , NO^\bullet , $^t\text{BuOOH}$, $\text{O}_2^{\bullet-}$, $^1\text{O}_2$, $^\bullet\text{OH}$, and HOCl). (b) PL titration of **Ir-1** (10 μ M) with HOCl (0–32.5 equiv).

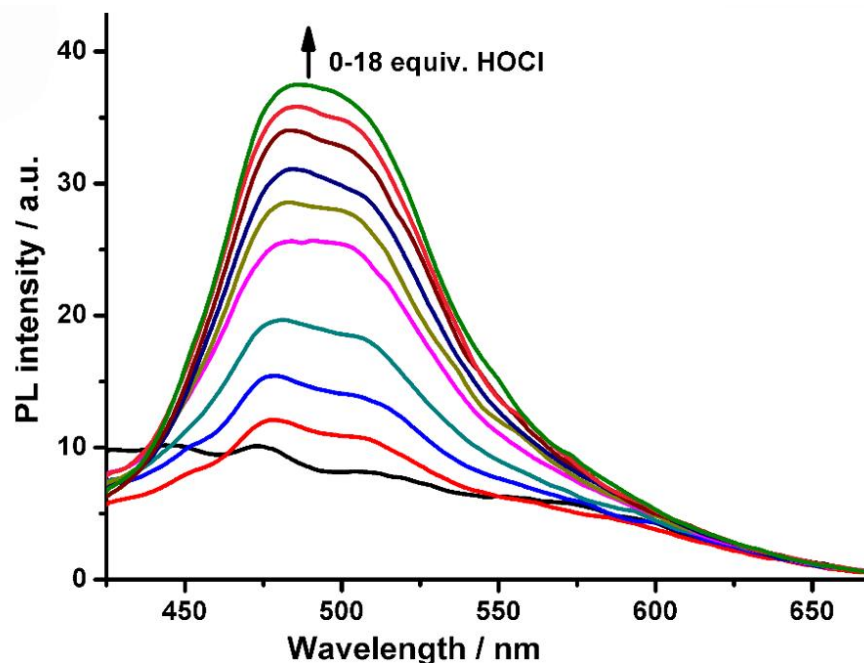
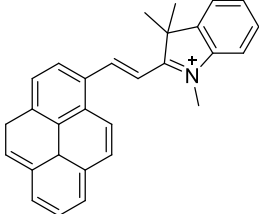
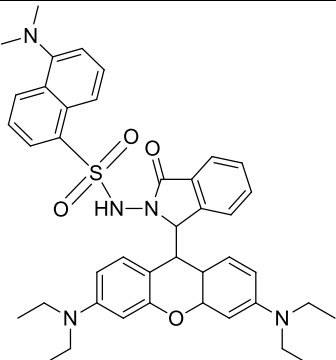
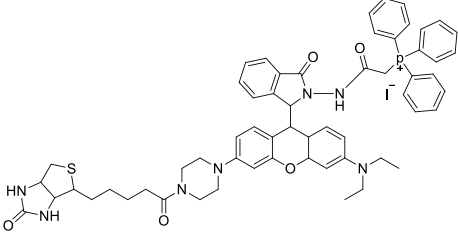
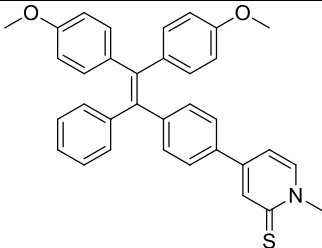
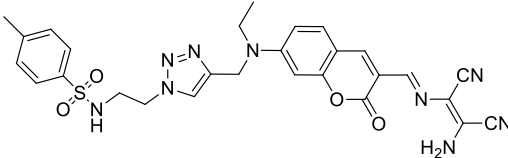
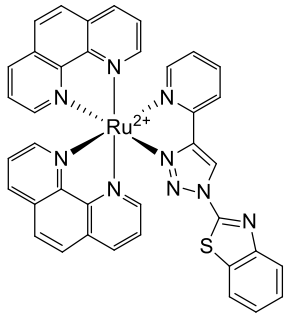
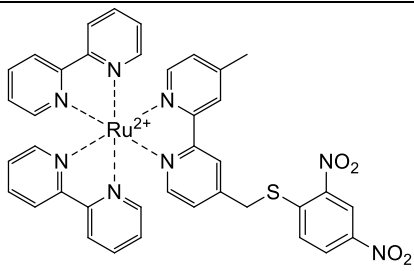
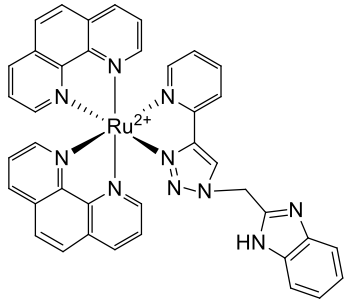
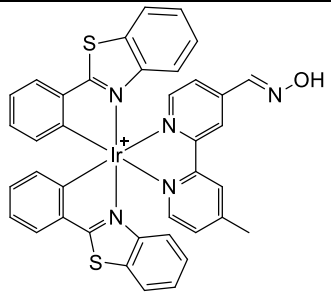
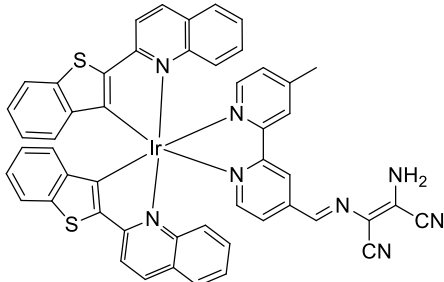
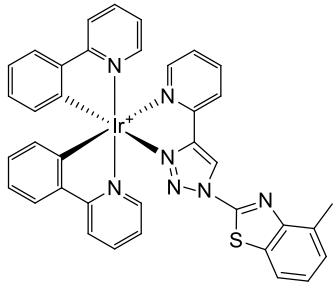


Fig. S9. PL titration of Ir-1 (10 μM) with HOCl (0-180 μM) for the determination of detection limit in PBS buffer (DMSO: PBS = 1:1, v/v).

Table S6. List of organic and inorganic probes and their respective detection limit and response time for the detection of HOCl.

Sl no.	Probe	Type	LOD	Response time	Reference
1.		Organic	0.35 μM	90 min	<i>ACS Appl. Mater. Interfaces</i> , 2016, 8 , 1511-1519.
2.		Organic	1.13 μM	1 min	<i>Inorg. Chem.</i> 2015, 54 , 8644-8649.

3.		Organic	0.21 μM	10 sec	<i>Chem Commun.</i> , 2017, 53 , 5539-5541
4.		Organic	92 nM	1 min	<i>Chem Commun.</i> , 2017, 53 , 11654-11657.
5.		Organic	0.59 μM	30 sec	<i>Chem Commun.</i> , 2019, 55 , 2533-2536.
6.		Inorganic	76 nM	18 min	<i>Inorg. Chem.</i> 2019, 58 , 9982-9991.
7.		Inorganic	53 nM	Not mentioned	<i>Inorg. Chem.</i> 2013, 52 , 10325-10331.
8.		Inorganic	7.5 μM	4 min	<i>Chemistry Select</i> , 2023, 3 , e202204643

9.		Inorganic	23.1 nM	1 min	<i>Anal. Chem.</i> , 2020, 92 , 8285-8291.
10.		Inorganic	27.7 nM	1.5 min	<i>Anal. Chem.</i> , 2021, 93 , 4628-4634.
11.		Inorganic	5.18 μM	30 sec	<i>Present work</i>

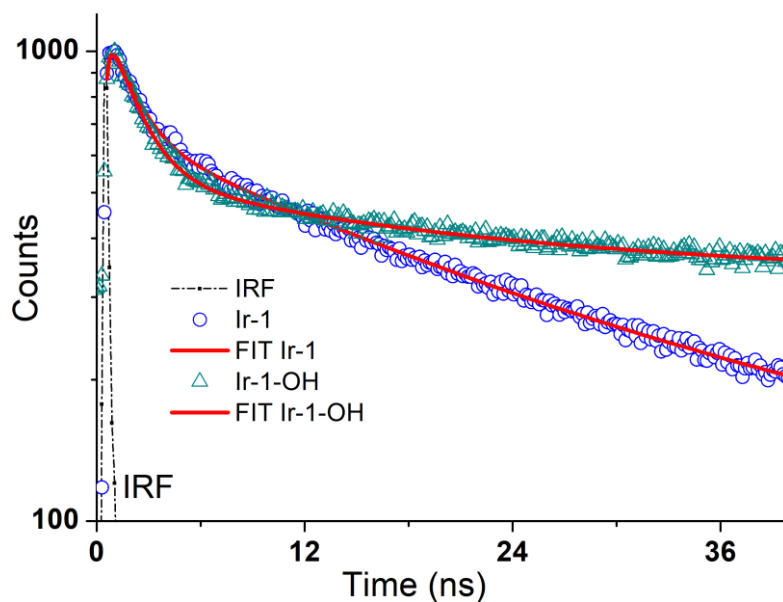


Fig. S10. Time-resolved emission decays of Ir-1 (10 μM) in the absence and presence of HOCl in PBS buffer (DMSO: PBS = 1:1, v/v).

Computational Study.

Density functional theory (DFT) and time-dependent-density functional theory (TD-DFT) calculations were performed to obtain insight into the electronic transitions responsible for the absorption spectra and luminescence spectra of **Ir-1** and **Ir-1-OH**. The energy optimized structures and selected theoretical bond lengths and angles are shown in Figure S11 and Table S6. The Cartesian coordinates for **Ir-1** and **Ir-1-OH** are given in Tables S7 and S8.

The theoretically obtained vertical excitation energies and composition of the related $^1\text{MLCT}$ transition assigned to the experimental UV-vis spectrum in water are displayed in Table S9. It is shown from the DFT calculations that the highest occupied MOs of **Ir-1** and **Ir-1-OH** are $d\pi$, $L1\pi$ and $\text{Ir}(d_{z^2})$ in character. Whereas, the lowest unoccupied MOs of **Ir-1** and **Ir-1-OH** are centred at the $L1\pi^*$ orbital of the ligand. The TD-DFT calculations for **Ir-1** indicate that the experimental $^1\text{MLCT}$ absorption band at ~ 317 nm (3.91 eV) arises from strong transitions characterized as $\text{HOMO-2} \rightarrow \text{LUMO+1}$, $\text{HOMO-3} \rightarrow \text{LUMO+1}$, and $\text{HOMO-7} \rightarrow \text{LUMO}$ ($f = 0.295$) (319 nm, 3.88 eV). In **Ir-1-OH**, the calculated strong transition at 298 nm (4.15 eV), which is due to the $\text{HOMO-3} \rightarrow \text{LUMO+1}$ and $\text{HOMO-8} \rightarrow \text{LUMO}$ transitions ($f = 0.22$), is assigned to the experimental absorption band at ~ 293 nm. After HOCl stimulated hydroxylation of **L1** ligand, the ppy ligand-based LUMO (π^*) is destabilized by 0.06 eV, causing a shift in the absorption in the lower wavelength region (Figure S12; Table S9)

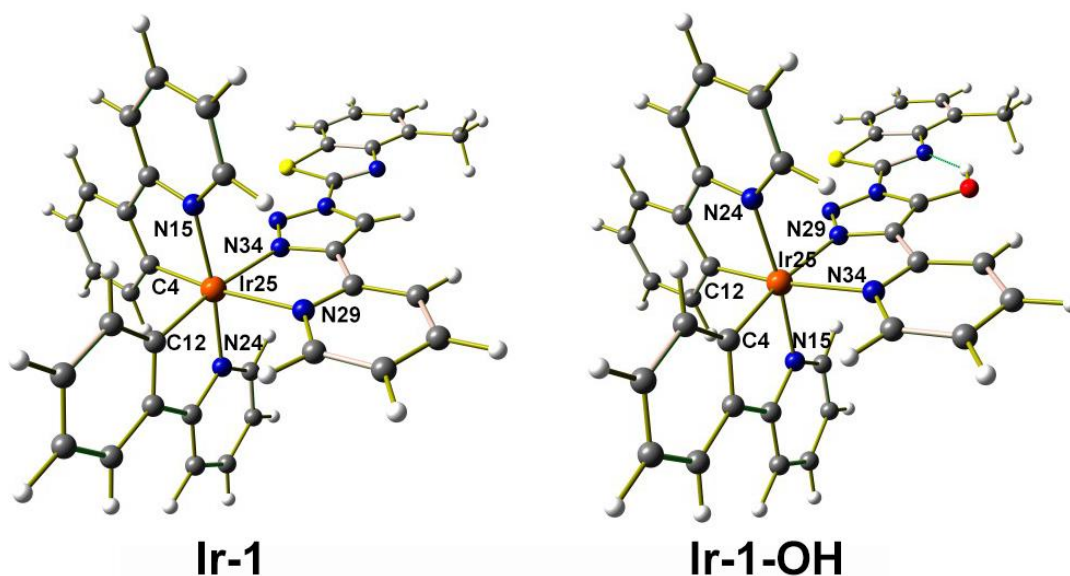


Fig. S11. Optimized structures of **Ir-1** and **Ir-1-OH** obtained from TD-DFT calculation at UB3LYP/6-31G+(d) / LANL2DZ.

Table S7. Selected Bond Lengths (Å) and bond angles (°) around the Ir(III) center in **Ir-1** and **Ir-1-OH** obtained from ground state DFT calculation.

For Ir-1			
Bond Lengths (Å)			
N(15)-Ir(25)	2.041	N(34)-Ir(25)	1.958
N(29)-Ir(25)	1.988	N(24)-Ir(25)	1.976
C(12)-Ir(25)	2.017	C(4)-Ir(25)	1.960
Bond angles (°)			
N(15)-Ir(25)-N(34)	82.66	N(34)-Ir(25)-N(29)	73.93
N(29)-Ir(25)-N(24)	80.94	N(24)-Ir(25)-C(12)	75.45
N(15)-Ir(25)-C(4)	71.20	C(4)-Ir(25)-C(12)	89.15

For Ir-1-OH			
Bond Lengths (Å)			
N(24)-Ir(25)	1.977	N(29)-Ir(25)	1.987
N(34)-Ir(25)	1.956	N(15)-Ir(25)	2.041
C(4)-Ir(25)	1.961	C(12)-Ir(25)	2.017
Bond angles (°)			
N(24)-Ir(25)-N(29)	80.86	N(29)-Ir(25)-N(34)	73.78
C(4)-Ir(25)-N(15)	71.22	N(24)-Ir(25)-C(12)	75.43
N(34)-Ir(25)-N(15)	83.36	C(4)-Ir(25)-C(12)	88.79

Table S8. Cartesian coordinates of **Ir-1** in the ground state.

	x	y	z		x	y	z
C	0.4516	-4.3551	0.0135	S	-4.4642	-2.5605	1.3768
C	0.5743	-3.8143	-1.2058	C	-6.2532	-2.3925	1.5901
C	0.6913	-2.4842	-1.2989	C	-6.5797	-1.1163	1.3173
C	0.7036	-1.7606	-0.1722	N	-5.5934	-0.2427	0.9718
C	0.6029	-2.2259	1.0671	C	-7.1343	-3.3316	1.9457
C	0.4626	-3.5739	1.1064	C	-8.4184	-2.9487	2.0283
C	3.6387	-0.0748	0.5436	C	-8.7725	-1.6796	1.7567
C	4.9461	-0.0942	0.2464	C	-7.8695	-0.7445	1.3999
C	5.3397	0.0958	-1.0215	C	-8.2884	0.6729	1.0875
C	4.4313	0.299	-1.9897	H	0.3408	-5.4488	0.1146
C	3.1167	0.3179	-1.7027	H	0.5578	-4.4457	-2.1113
C	2.7372	0.1355	-0.4274	H	0.7593	-2.0117	-2.2893
C	0.6085	-1.7921	2.3419	H	0.3604	-4.1061	2.0713
C	2.0927	0.4934	-2.5619	H	3.325	-0.2387	1.5848
N	0.7983	-0.5395	1.8105	H	5.6932	-0.2698	1.0406
C	1.0117	0.5979	2.3492	H	6.4154	0.0766	-1.2693
C	1.0376	0.9771	3.6187	H	4.8114	0.4398	-3.0139
C	0.7813	-0.1204	4.3038	H	1.2208	1.395	1.6299
C	0.6343	-1.2297	3.5688	H	1.2296	1.9875	4.0188
C	2.237	0.6919	-3.8873	H	0.7319	-0.1101	5.4076
C	1.1582	0.8346	-4.6724	H	0.4669	-2.0762	4.2579
C	-0.0512	0.7675	-4.102	H	3.222	0.7397	-4.3772
C	-0.0942	0.5709	-2.7768	H	1.2602	0.9968	-5.7597
N	0.9313	0.4473	-2.0445	H	-0.9726	0.8714	-4.701
Ir	0.7487	0.1977	-0.0923	H	-1.0721	0.5079	-2.2773
C	-0.6451	4.6309	-0.3922	H	-0.9895	5.6764	-0.4675
C	0.6475	4.3197	-0.5665	H	1.3956	5.1005	-0.7861
C	1.0033	3.0298	-0.4663	H	2.0568	2.7394	-0.6003
N	0.182	2.0993	-0.2191	H	-2.5763	3.872	0.0297
C	-1.0451	2.3811	-0.0447	H	-3.9507	1.8634	0.5184
C	-1.5081	3.6399	-0.1215	H	-6.8229	-4.3679	2.1604
C	-1.8053	1.3089	0.2133	H	-9.188	-3.6855	2.3172
C	-3.1138	1.1478	0.4564	H	-9.8386	-1.4041	1.8311
N	-1.1824	0.2104	0.2311	H	-7.9163	1.3664	1.8755
N	-1.9825	-0.7215	0.4787	H	-7.8781	0.9973	0.1038
N	-3.2121	-0.1779	0.6291	H	-9.3949	0.7882	1.0306
C	-4.3593	-0.799	0.9324				

Table S9. Cartesian coordinates of **Ir-1-OH** in the ground state.

	x	y	z		x	y	z
C	0.4516	-4.3551	0.0135	S	-4.4642	-2.5605	1.3768
C	0.5743	-3.8143	-1.2058	C	-6.2532	-2.3925	1.5901
C	0.6913	-2.4842	-1.2989	C	-6.5797	-1.1163	1.3173
C	0.7036	-1.7606	-0.1722	N	-5.5934	-0.2427	0.9718
C	0.6029	-2.2259	1.0671	C	-7.1343	-3.3316	1.9457
C	0.4626	-3.5739	1.1064	C	-8.4184	-2.9487	2.0283
C	3.6387	-0.0748	0.5436	C	-8.7725	-1.6796	1.7567
C	4.9461	-0.0942	0.2464	C	-7.8695	-0.7445	1.3999
C	5.3397	0.0958	-1.0215	C	-8.2884	0.6729	1.0875
C	4.4313	0.299	-1.9897	H	0.3408	-5.4488	0.1146
C	3.1167	0.3179	-1.7027	H	0.5578	-4.4457	-2.1113
C	2.7372	0.1355	-0.4274	H	0.7593	-2.0117	-2.2893
C	0.6085	-1.7921	2.3419	H	0.3604	-4.1061	2.0713
C	2.0927	0.4934	-2.5619	H	3.325	-0.2387	1.5848
N	0.7983	-0.5395	1.8105	H	5.6932	-0.2698	1.0406
C	1.0117	0.5979	2.3492	H	6.4154	0.0766	-1.2693
C	1.0376	0.9771	3.6187	H	4.8114	0.4398	-3.0139
C	0.7813	-0.1204	4.3038	H	1.2208	1.395	1.6299
C	0.6343	-1.2297	3.5688	H	1.2296	1.9875	4.0188
C	2.237	0.6919	-3.8873	H	0.7319	-0.1101	5.4076
C	1.1582	0.8346	-4.6724	H	0.4669	-2.0762	4.2579
C	-0.0512	0.7675	-4.102	H	3.222	0.7397	-4.3772
C	-0.0942	0.5709	-2.7768	H	1.2602	0.9968	-5.7597
N	0.9313	0.4473	-2.0445	H	-0.9726	0.8714	-4.701
Ir	0.7487	0.1977	-0.0923	H	-1.0721	0.5079	-2.2773
C	-0.6451	4.6309	-0.3922	H	-0.9895	5.6764	-0.4675
C	0.6475	4.3197	-0.5665	H	1.3956	5.1005	-0.7861
C	1.0033	3.0298	-0.4663	H	2.0568	2.7394	-0.6003
N	0.182	2.0993	-0.2191	H	-2.5763	3.872	0.0297
C	-1.0451	2.3811	-0.0447	H	-3.9507	1.8634	0.5184
C	-1.5081	3.6399	-0.1215	H	-6.8229	-4.3679	2.1604
C	-1.8053	1.3089	0.2133	H	-9.188	-3.6855	2.3172
C	-3.1138	1.1478	0.4564	H	-9.8386	-1.4041	1.8311
N	-1.1824	0.2104	0.2311	H	-7.9163	1.3664	1.8755
N	-1.9825	-0.7215	0.4787	H	-7.8781	0.9973	0.1038
N	-3.2121	-0.1779	0.6291	H	-9.3949	0.7882	1.0306
C	-4.3593	-0.799	0.9324				

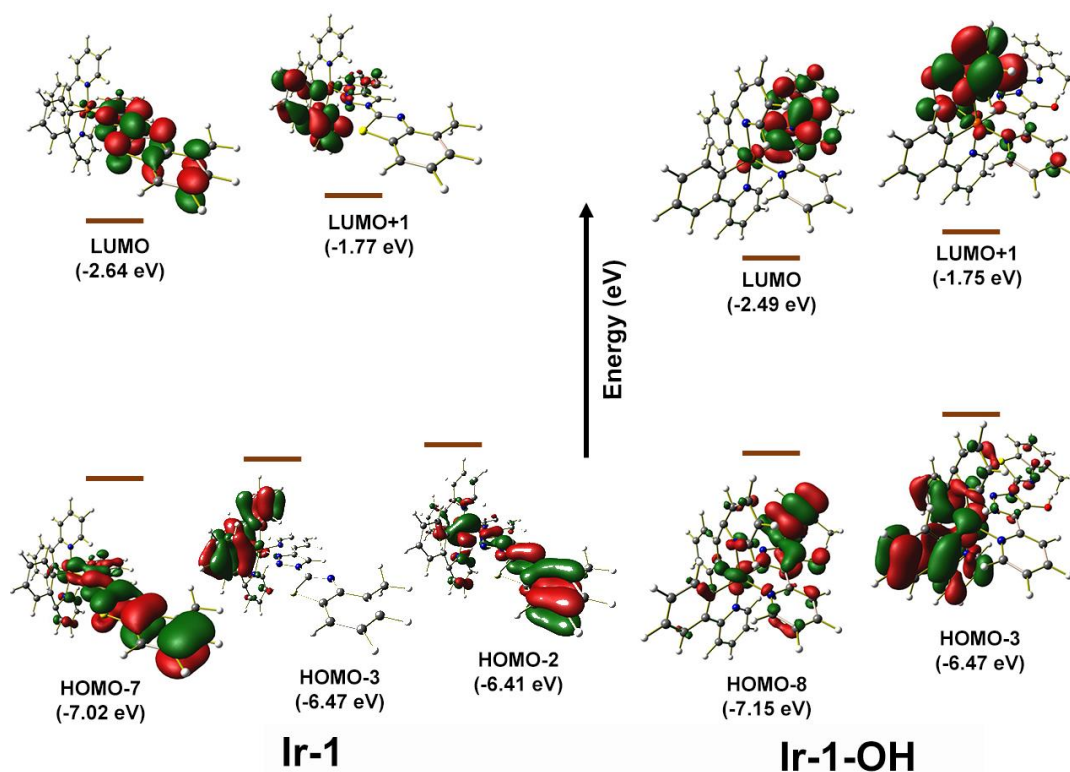


Fig. S12. Spatial plots of selected molecular orbitals of **Ir-1** and **Ir-1-OH**, obtained from singlet state TD-DFT calculation at UB3LYP/6-31G+(d) / LANL2DZ level using the optimized ground-state geometry in H₂O (isovalue = 0.03).

Table S10. Selected singlet state electronic transitions of **Ir-1** and **Ir-1-OH** obtained from TDDFT calculation at UB3LYP/6-31G+(d) / LANL2DZ level in H₂O.

Complex	Experimentally observed excitation energy [eV(nm)]	Computed vertical excitation transition [eV(nm)]	f^a	Transition	Assignment	C_I^b
Ir-1	317nm (3.91 eV)	319 nm (3.88 eV)	0.295	HOMO-2 \rightarrow LUMO+1	$^1MC/{}^1ILCT$	0.31
				HOMO-3 \rightarrow LUMO+1		0.10
				HOMO-7 \rightarrow LUMO		0.58
Ir-1-OH	293 nm (4.23 eV)	298 nm (4.15 eV)	0.22	HOMO-3 \rightarrow LUMO+1	$^1MC/{}^1LL'CT$	0.51
				HOMO-8 \rightarrow LUMO		0.11

^aoscillator strength, ^bcoefficients are in absolute values.

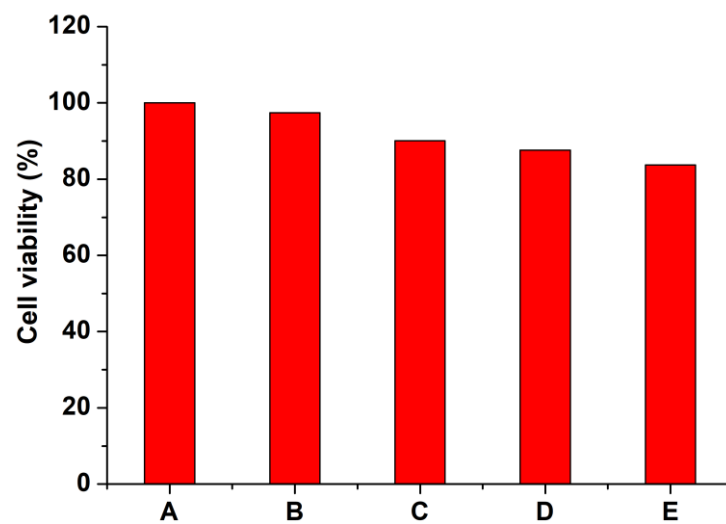


Fig. S13. Cell viability was assayed by MTT test with different concentrations of **Ir-1** (A: 0 μ M; B: 10 μ M, C: 25 μ M; D: 50 μ M; E: 100 μ M) in HEK-293T cells.